Mathematical imaging

Habib Ammari

Department of Mathematics, ETH Zürich

Mathematics for biomedical imaging

- Biomedical imaging:
  - Image electrical, optical, and mechanical tissue properties using electromagnetic and elastic waves at single or multiple frequencies.
  - Enhance the resolution, the stability, and the specificity.
- Direct and inverse problems for wave propagation in complex media.
- Build mathematical frameworks and develop effective numerical algorithms for biomedical imaging applications.

Mathematics for biomedical imaging

- Key concepts:
  - Resolution: smallest detail that can be resolved.
  - Robustness: stability of the image formation with respect to model uncertainty and electronic noise.
  - Specificity: physical nature (benign or malignant for tumors).

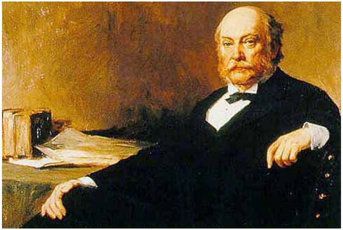

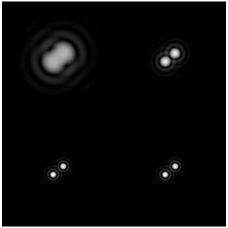

Mathematics for biomedical imaging

- Waves play a key role in biomedical imaging techniques.
- Visualize contrast information on the electrical, optical, mechanical properties of tissues.
- Tissue contrasts:
  - Highly sensitive to physiological and pathological tissue status.
  - Depend on the cell organization and composition.
  - Overall parameters, averaged in space over many cells.
- Recognize the microscopic cell organization and composition from measurements at the macroscopic level.

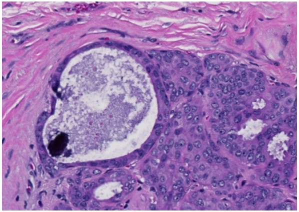

Mathematics for biomedical imaging

- Diagnosis and staging of cancer disease.
- Help surgeons to make sure they removed everything unwanted around the margin of the cancer tumor.
- Perform biopsy in the operating room.

Mathematics for biomedical imaging

- Anomaly imaging: take advantage of the smallness of the imaged anomalies.
- Hybrid imaging: one single imaging system based on the combined use of conductivity imaging and acoustic or elastic waves.
    - Conductivity imaging: sensitivity to only the electrical contrast.
    - Spatial resolution: low.
    - Hybrid imaging: Conductivity imaging gives its contrast and acoustic or elastic wave its spatial resolution.
- Spectroscopic tissue property imaging: specific dependence with respect to the frequency of the contrast.
    - Detect the characteristic signature of tumors; determine which are malignant and which are benign: specificity enhancement.
    - Classify micro-structure organization using spectroscopic tissue property imaging: resolution enhancement.
- Single particle imaging: take advantage of scattering and absorption enhancements and single particle imaging.

Mathematics for biomedical imaging

- Anomaly imaging:
  - Conductivity anomalies.
- Hybrid imaging:
  - Acousto-electric effect:
  - Ultrasound-modulated optical tomography;
  - Full-field optical coherence elastography
- Spectroscopic imaging:
  - Spectroscopic electrical tissue property imaging.
- Single particle imaging:
  - Plasmonic nanoparticles.

Scale-Separation techniques

- Scale separation techniques: take advantage of the smallness of the imaged anomalies.
- Conductivity anomaly D inside a background medium Ω.
- k: conductivity of D; 1: background conductivity.
- $\lambda = (k+1)/(2(k-1))$: conductivity contrast.
- Detect, localize, and characterize the anomaly D from boundary measurements on $\partial\Omega$.

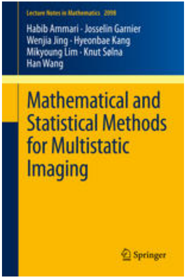

Scale-Separation techniques

- Use multipolar approximation:

$$u(x) - U(x) \simeq \sum_{\alpha,\beta} \partial^\alpha G(x-z) M_{\alpha\beta}(\lambda, D) \partial^\beta U(z).$$

- u: voltage potential with D; U: voltage potential without D.
- G: background Green's function.
- $M_{\alpha\beta}(\lambda, D)$: high-order polarization tensors.

$$M_{\alpha\beta}(\lambda, D) := \int_{\partial D} x^\beta (\lambda I - \mathcal{K}_D^*)^{-1}[\partial x^\alpha / \partial \nu](x)\, ds(x).$$

Scale-Separation techniques

- Neumann-Poincaré operator $\mathcal{K}_D^*$:

$$\mathcal{K}_D^*[\varphi](x) := \int_{\partial D} \frac{\partial G}{\partial \nu(x)}(x-y)\varphi(y)\, ds(y) \ , \quad x \in \partial D.$$

  ν: normal to ∂D.

- G: Fundamental solution to the Laplacian.
- $\mathcal{K}_D^*$: compact operator on $L^2(\partial D)$; Spectrum of $\mathcal{K}_D^*$ lies in $(-\frac{1}{2}, \frac{1}{2}]$ (Kellog).
- Spectral decomposition formula in $H^{-1/2}(\partial D)$,

$$\mathcal{K}_D^*[\psi] = \sum_{j=0}^{\infty} \lambda_j (\psi, \varphi_j)_{\mathcal{H}^*} \varphi_j.$$

- (λ_j, φ_j), $j = 0, 1, 2, \ldots$: eigenvalue and normalized eigenfunction pair of $\mathcal{K}_D^*$ in $\mathcal{H}^*(\partial D)$; $\lambda_j \in (-\frac{1}{2}, \frac{1}{2}]$ and $\lambda_j \to 0$ as $j \to \infty$;
- $\mathcal{H}^*(\partial D) = H^{-\frac{1}{2}}(\partial D)$ equipped with

$$(u, v)_{\mathcal{H}^*} = -(u, \mathcal{S}_D[v])_{-\frac{1}{2}, \frac{1}{2}}; \quad \mathcal{S}_D : \text{single layer potential.}$$

Scale-Separation techniques

Properties of high-order polarization tensors:

- Recover high-frequency information on the shape;
- Separate topology;
- Determine uniquely the shape and the material parameter.

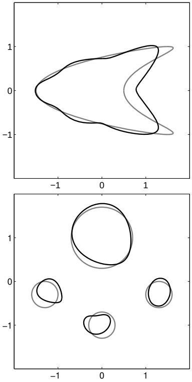

Scale-Separation techniques

- Positivity and symmetry properties on harmonic coefficients; optimal bounds.
- Harmonic coefficients:

$$(x_1 + ix_2)^m = \sum_{|\alpha|=m} a_\alpha^m x^\alpha + i \sum_{|\beta|=m} b_\beta^m x^\beta.$$

- Translation, rotation, and scaling formulas.

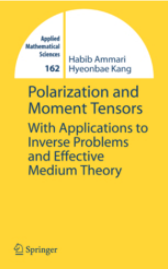

Scale-Separation techniques

- Location-search algorithms: subspace projection algorithms.
- P_m orthogonal projection onto the m first significant singular values of data matrix.
- MUltiple SIgnal Classification algorithm:

$$\mathcal{I}_{MU}(z^s) = 1 \Big/ \sqrt{1 - \sum_{|\alpha| \leq 1} \|(I - P_m)(\partial^\alpha G(\cdot, z^s))\|}.$$

- $\mathcal{I}_{MU}(z^s)$ peaks at the location of the anomaly.

Scale-Separation techniques

- MUSIC Imaging functional: MUSIC-type reconstruction from the singular value decomposition of data matrix.

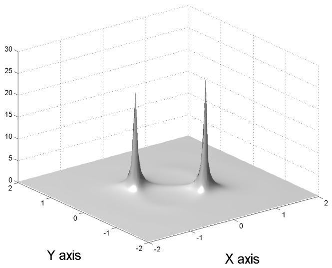

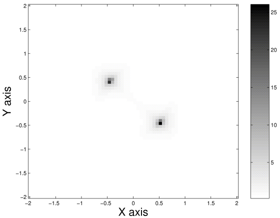

Scale-Separation techniques

- Reconstruction of high-order polarization tensors from the data by a least squares method.
- Instability:

$$M_{\alpha\beta}(k, D) = O(|D|^{|\alpha|+|\beta|+d-2}), |\partial^\alpha G(x-z)| = O(|x|^{-|\alpha|})(|x| \to +\infty).$$

- Resolving power= number of high-order polarization tensors reconstructed from the data: depends on the signal-to-noise ratio (SNR) in the data.
- $\epsilon =$ characteristic size of the anomaly/ the distance to the boundary $\partial\Omega$.
- $\mathrm{SNR} = \epsilon^2$/standard deviation of the measurement noise (Gaussian).
- Formula for the resolving power m as function of the SNR:

$$(m\epsilon^{1-m})^2 = \mathrm{SNR}.$$

Hybrid techniques

- Hybrid imaging: one single imaging system based on the combined use of different imaging modalities.

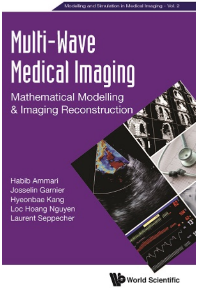

Acousto-electric imaging

- Acousto-electric effect:
  - Acoustic pressure: $p(x,t) = p_0 b(x) a(t)$; p_0: amplitude; b: beam pattern; a: ultrasound waveform.
  - Acousto-electric effect:

$$\Delta\sigma = \eta\sigma p; \quad \eta: \text{ interaction constant.}$$

- Acousto-electric imaging:
  - Change of conductivity induces a change of the boundary voltage measurements.
  - Scan the sample, record the boundary variations, and determine the conductivity distribution.

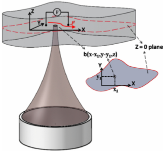

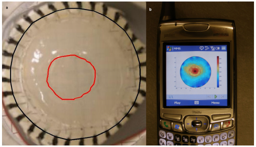

Acousto-electric imaging

- Acousto-electric imaging: mathematical and numerical framework[1].
- u the voltage potential induced by a current g in the absence of acoustic perturbations:

$$\left\{ \begin{array}{l} \nabla_x \cdot (\sigma(x) \nabla_x u) = 0 \text{ in } \Omega \, , \\ \displaystyle \sigma(x) \frac{\partial u}{\partial \nu} = g \text{ on } \partial\Omega \, . \end{array} \right.$$

- Suppose σ bounded from below and above and known in a neighborhood of the boundary $\partial\Omega$: $\sigma = \sigma_\star$; Set $\Omega' \subset \Omega$ where σ is unknown.

[1] with E. Bonnetier, Y. Capdeboscq, M. Fink, M. Tanter, SIAM J. Appl. Math., 2008.

Acousto-electric imaging

- Use of focalized ultrasonic waves with D as a focal spot $\rightarrow$

$$\sigma_\delta(x) \quad = \quad \sigma(x)\Big[1 + \chi(D)(x)\,(\nu(x) - 1)\Big],$$

with $\nu(x) = \eta p(x)$: known.

- u_δ induced by g in the presence of acoustic perturbations localized in the focal spot $D := z + \delta B$:

$$\left\{ \begin{array}{l} \nabla_x \cdot (\sigma_\delta(x)\nabla_x u_\delta(x)) = 0 \text{ in } \Omega, \\ \qquad \sigma(x)\dfrac{\partial u_\delta}{\partial \nu} = g \text{ on } \partial\Omega. \end{array} \right.$$

Acousto-electric imaging

- Suppose the focal spot D to be a disk and $u \in W^{2,\infty}(D)$. Then,

$$\int_{\partial\Omega} (u_\delta - u) g \, d\sigma = |\nabla u(z)|^2 \int_D \sigma(x) \frac{(\nu(x)-1)^2}{\nu(x)+1} dx$$
$$+ O(|D|^{1+\beta}),$$

  - $O(|D|^{1+\beta}) \leq C |D|^{1+\beta} ||\nabla u||_{L^\infty(D)} |\nabla^2 u||_{L^\infty(D)}$ with C: independent of D and u.
  - β: depends only on Ω', ν, $\sup_\Omega \sigma, \min_\Omega \sigma$.

Acousto-electric imaging

- Suppose $\sigma \in \mathcal{C}^{0,\alpha}(D)$, $0 \leq \alpha \leq 2\beta \leq 1$. Then

$$\begin{aligned} \mathcal{E}(z) &:= \left(\int_D \frac{(\nu(x) - 1)^2}{\nu(x) + 1} dx \right)^{-1} \int_{\partial\Omega} (u_\delta - u) g \, d\sigma \\ &= \sigma(z) \left| \nabla u(z) \right|^2 + O(|D|^{\alpha/2}). \end{aligned}$$

- $\mathcal{E}(z)$: electrical energy density; known function from the boundary measurements.

Acousto-electric imaging

- Substitute σ by $\mathcal{E}/\left|\nabla u\right|^2$.
- Nonlinear PDE (the 0–Laplacian)

$$\left\{ \begin{aligned} \nabla_x \cdot \left(\frac{\mathcal{E}}{\left|\nabla u\right|^2} \nabla u \right) = 0 \quad & \text{in } \Omega \, , \\ \frac{\mathcal{E}}{\left|\nabla u\right|^2} \frac{\partial u}{\partial \nu} = g \quad & \text{on } \partial\Omega \, . \end{aligned} \right.$$

- g such that u has no critical point inside Ω'.

Acousto-electric imaging

- Polarized measurements:
- g_1 and g_2: two currents.

$$\mathcal{E}_{ij} := \int_{\partial\Omega} (u_\delta^{(j)} - u^{(j)}) g_i \, d\sigma \approx \sigma(x) \nabla u^{(j)}(x) \cdot \nabla u^{(l)}(x), \quad i,j = 1,2.$$

- $$\begin{cases} \nabla_x \cdot \left(\dfrac{\mathcal{E}_{jj}}{|\nabla u^{(j)}|^2} \nabla u^{(j)} \right) = 0 & \text{in } \Omega\,, \\ \dfrac{\mathcal{E}_{jj}}{|\nabla u^{(j)}|^2} \dfrac{\partial u^{(j)}}{\partial \nu} = g_j & \text{on } \partial\Omega\,. \end{cases}$$

- Proper set of measurements: (g_1, g_2) s.t.

$$|\nabla u^{(j)}| > 0; (\mathcal{E}_{ij})_{i,j} : \text{ invertible in } \Omega' \Subset \Omega.$$

Acousto-electric imaging

- Substitution algorithm.
  - Start from an initial guess for the conductivity σ;
  - Solve the corresponding Dirichlet conductivity problem

$$\begin{cases} \nabla \cdot (\sigma \nabla u_0) = 0 & \text{in } \Omega \,, \\ u_0 = \psi & \text{on } \partial\Omega \,. \end{cases}$$

  - ψ: Dirichlet data measured as a response to the current $g = g_1$ in absence of elastic deformation;
  - Define the discrepancy between the data and the guessed solution by

$$\epsilon_0 := \frac{\mathcal{E}_{11}}{|\nabla u_0|^2} - \sigma \,.$$

Acousto-electric imaging

- Introduce the corrector, δu, computed as the solution to

$$\begin{cases} \nabla \cdot (\sigma \nabla \delta u) = -\nabla \cdot (\varepsilon_0 \nabla u_0) & \text{in } \Omega \,, \\ \delta u = 0 & \text{on } \partial\Omega \,; \end{cases}$$

- Update the conductivity

$$\sigma := \frac{\mathcal{E}_{11} - 2\sigma \nabla \delta u \cdot \nabla u_0}{|\nabla u_0|^2} \,.$$

- Iteratively update the conductivity, alternating directions of currents (with $g = g_2$ and $\mathcal{E}_{11}$ replaced with $\mathcal{E}_{22}$).

Acousto-electric imaging

- Optimal control algorithm
- (g_1, g_2): proper set of measurements.
- Admissible set of conductivities: open subset of $W^{1,\infty}(\Omega)$

$$A = \{\sigma \in W^{1,2}(\Omega) : c_0 < \sigma < C_0, |\nabla \sigma| < C_1\} .$$

- Minimization problem:

$$\min_{\sigma \in A} J[\sigma] := \frac{1}{2} \sum_{j,l=1}^{2} \int_{\Omega} \left| \mathcal{E}_{jl}[\sigma] - \mathcal{E}_{jl}^{(m)} \right|^2 dx ,$$

$\mathcal{E}_{jl}^{(m)}$: measurements.

Acousto-electric imaging

- Fréchet derivative of $J[\sigma]$:

$$dJ[\sigma] = \frac{1}{2}\sum_{j,l=1}^{2}(\mathcal{E}_{jl}[\sigma] - \mathcal{E}_{jl}{}^{(m)})\nabla u^{(j)} \cdot \nabla u^{(l)} + \sum_{j,l=1}^{2} \nabla u^{(j)} \cdot \nabla p^{(j,l)}\,;$$

- $p^{(j,l)}$: solution of the adjoint problem

$$\left\{\begin{array}{rcll} \nabla \cdot \sigma \nabla p^{(j,l)} & = & -\nabla \cdot (\mathcal{E}_{jl}[\sigma] - \mathcal{E}_{jl}^{(m)})\sigma \nabla u^{(l)} & \text{in } \Omega\,, \\ \sigma \frac{\partial p^{(j,l)}}{\partial \nu} & = & 0 & \text{on } \partial\Omega\,, \\ \displaystyle\int_{\partial\Omega} p^{(j,l)} = 0\,. & & & \end{array}\right.$$

Acousto-electric imaging

- For $\sigma \in A$, $d\mathcal{E}_{jl}$ takes the form $I + \mathrm{compact}$, up to a multiplication by a continuous function.
- $\Rightarrow$
$$\|d\mathcal{E}[\sigma]\|_{\mathcal{L}(H^1_0(\Omega),L^2(\Omega))} \geq C\,.$$
- Convergence of the Landweber iteration scheme:
  - Assume that $\sigma^{(0)}$: good initial guess for σ_*.
  - As $n \to +\infty$, the sequence
$$\sigma^{(n+1)} = T\sigma^{(n)} - \eta d\mathcal{E}^*[T\sigma^{(n)}](\mathcal{E}[\sigma^{(n)}] - \mathcal{E}^{(m)})$$
    converges to σ_*; T: Hilbert projection of $H^1(\Omega)$ onto A; σ_*: true conductivity distribution, η: step size; $\mathcal{E}^{(m)} = (\mathcal{E}_{jl}^{(m)})_{j,l=1,2}$.

Acousto-electric imaging

Reconstruct the conductivity distribution knowing the internal energies:

- Linearized versions of the nonlinear (zero-Laplacian) PDE problems.
- Optimal control approach: minimize over the conductivity the discrepancy between the computed and reconstructed internal energies.
- Optimal control approach: more efficient approach specially with incomplete internal measurements of the internal energy densities.
- Resolution of order the size of the focal spot + stability (wrt measurement noise).
- Exact inversion formulas: derivatives of the data $\Rightarrow$ used only to obtain a good initial guess.

- Reconstruction algorithm for ultrasound-modulated diffuse optical tomography.
- Diffuse optical imaging: low resolution.
- By mechanically perturbing the medium → achieve a significant resolution enhancement.
    - Spherical acoustic wave: propagating inside the medium → optical parameter of the medium: perturbed.
    - Cross-correlations of the boundary measurements of the intensity of the light propagating in the perturbed medium and in the unperturbed one → two iterative algorithms for reconstructing the optical absorption coefficient:
        - Spherical Radon transform inversion → nonlinear system: solved iteratively or by optimal control.

Ultrasound-modulated optical tomography

- Acoustically modulated optical tomography[2]:

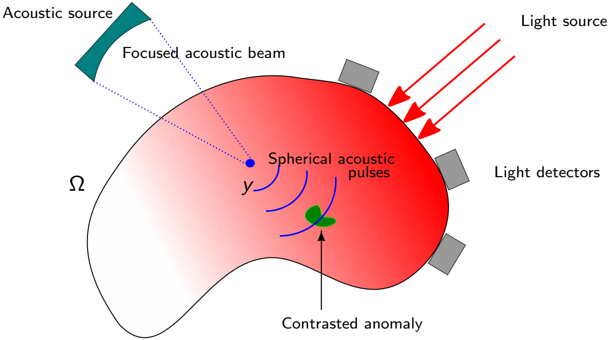

- Record the variations of the light intensity on the boundary due to the propagation of the acoustic pulses.

[2] with E. Bossy, J. Garnier, L. Nguyen, L. Seppecher, Proc. AMS, 2014.

Ultrasound-modulated optical tomography

- g: the light illumination; a: optical absorption coefficient; l: extrapolation length. Fluence Φ (in the unperturbed domain):

$$\begin{cases} -\Delta\Phi + a\Phi = 0 \quad \text{in } \Omega, \\ \displaystyle l\frac{\partial\Phi}{\partial\nu} + \Phi = g \quad \text{on } \partial\Omega. \end{cases}$$

- Acoustic pulse propagation: $a \to a_u(x) = a(x + u(x))$.
- Fluence Φ_u (in the displaced domain):

$$\begin{cases} -\Delta\Phi_u + a_u\Phi_u = 0 \quad \text{in } \Omega, \\ \displaystyle l\frac{\partial\Phi_u}{\partial\nu} + \Phi_u = g \quad \text{on } \partial\Omega. \end{cases}$$

- u: thin spherical shell growing at a constant speed; y: source point; r: radius.
- Cross-correlation formula:

$$M(y,r) := \int_{\partial\Omega}\left(\frac{\partial\Phi}{\partial\nu}\Phi_u - \frac{\partial\Phi_u}{\partial\nu}\Phi\right) = \int_{\Omega}(a_u - a)\Phi\Phi_u \approx \underbrace{\int_{\Omega} u \cdot \nabla a\,|\Phi|^2}_{Taylor+Born}.$$

Ultrasound-modulated optical tomography

- Helmholtz decomposition: $\Phi^2 \nabla a = \nabla \psi + \nabla \times A$.
- Spherical Radon transform: $\nabla \psi = -\frac{1}{c} \nabla \mathcal{R}^{-1} \left[\int_0^r \frac{M(y,\rho)}{\rho^{d-2}} d\rho \right]$.
- System of nonlinearly coupled elliptic equations: $\nabla \cdot \Phi^2 \nabla a = \Delta \psi$ and $\Delta \Phi + a \Phi = 0$.
- Fixed point and Optimal control algorithms.
- Convergence result for the fixed point scheme provided that $\|\Delta \psi\|_{L^\infty(\Omega)}$: small.

Ultrasound-modulated optical tomography

- Optimal control and Landweber schemes:
  - $F[a] := \nabla \cdot (\Phi^2[a]\nabla a)$;
  - Optimal control: $\min \|F[a] - \Delta\psi\|$;
  - Landweber sequence:

$$a^{(n+1)} = a^{(n)} - \mu dF[a^{(n)}]^*(F[a^{(n)}] - \Delta\psi),$$

  - $\mu > 0$: relaxation parameter.
  - Convergence results assuming a good initial guess.
  - $dF[a]$: well-defined on $H_0^1(\Omega)$ and there exists a positive constant C s.t. for all $h \in H_0^1(\Omega)$,

$$\|dF[a](h)\|_{H^{-1}(\Omega)} \geq C\|h\|_{H_0^1(\Omega)}.$$

$$dF[a](h) : v \in H_0^1(\Omega) \mapsto dF[a](h, v).$$

Ultrasound-modulated optical tomography

Realistic biological light absorption map:

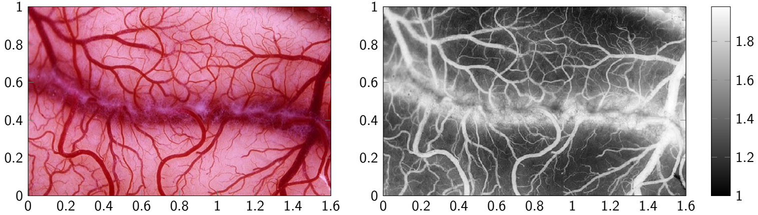

Ultrasound-modulated optical tomography

- Reconstruction for a realistic absorption map: proofs of convergence for highly discontinuous absorption maps[3] (bounded variation).
- Minimal regularity assumption on a (SBV^∞; change of function):

$$\widetilde{a} := a - a_0 - \frac{\psi}{\phi^2}.$$

- a and ψ: same set of discontinuities.

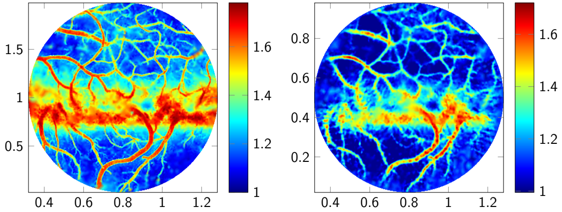

[3] with L. Nguyen, L. Seppecher, J. Funct. Anal., 2014.

Full-field optical coherence elastography

- Full-field optical coherence tomography (OCT): optical image with sub-cellular resolution.
- Elastography: mechanical tissue properties.
- Biological tissues: quasi-incompressible.
- Apply a load on the sample.
- OCTE: Use a set of optical images before and after mechanical solicitation to reconstruct the shear modulus distribution inside the sample.
- Map of mechanical properties: added as a supplementary contrast mechanism to enhance specificity.

Full-field optical coherence elastography

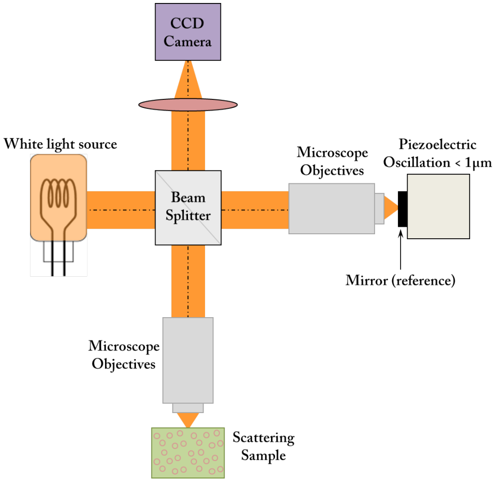

Full-field optical coherence elastography

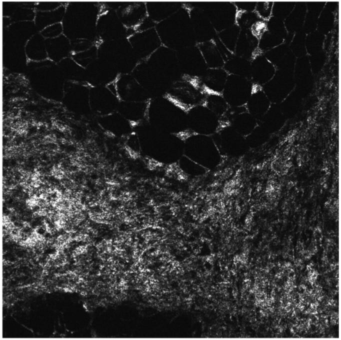

Full-field optical coherence elastography

- Reconstruct the shear modulus μ from ε and ε_u[4].
- $\varepsilon(\mathbf{x}) = \varepsilon_u\left(\mathbf{x} + \mathbf{u}(\mathbf{x})\right);$
- Displacement field $\mathbf{u}$:

$$\left\{ \begin{aligned} \nabla \cdot \left(\mu(\nabla \mathbf{u} + \nabla \mathbf{u}^T)\right) + \nabla p = 0 & \quad \text{in} \quad \Omega, \\ \nabla \cdot \mathbf{u} = 0 & \quad \text{in} \quad \Omega, \\ \mathbf{u} = \mathbf{f} & \quad \text{on} \quad \partial\Omega. \end{aligned} \right.$$

[4] with E. Bretin, P. Millien, L. Seppecher, J.K. Seo, SIAM J. Appl. Math., 2015.

Full-field optical coherence elastography

- $\mathbf{u}^*$ the true displacement; $\widetilde{\varepsilon}$ the measured deformed optical:

$$\widetilde{\varepsilon} = \varepsilon \circ (\mathbb{I} + \mathbf{u}^*)^{-1}.$$

- Optical image: discontinuous.
- Optimal control algorithm:

$$I(\mathbf{u}) = \frac{1}{2} \int_\Omega |\widetilde{\varepsilon} \circ (\mathbb{I} + \mathbf{u}) - \varepsilon|^2 \, d\mathbf{x}.$$

- I has a nonempty subgradient.
- $\boldsymbol{\xi} \in \partial I$:

$$\boldsymbol{\xi} : \mathbf{h} \mapsto \int_\Omega [\widetilde{\varepsilon}(\mathbf{x} + \mathbf{u}) - \varepsilon(\mathbf{x})]\mathbf{h}(\mathbf{x}) \cdot D\widetilde{\varepsilon} \circ (\mathbb{I} + \mathbf{u})(\mathbf{x}) \, d\mathbf{x}.$$

Full-field optical coherence elastography

Initial guess:

- Detect the surface of jumps of the optical image (edge detection algorithm).
- Local recovery by linearization: $\mathrm{data} = \varepsilon - \varepsilon_u (\approx \nabla\varepsilon \cdot \mathbf{u})$

$$J_{\mathbf{x}}(\mathbf{u}) = \int_\Omega |\nabla\varepsilon(\mathbf{y}) \cdot \mathbf{u} - \mathrm{data}(\mathbf{y})|^2 w_\delta(|\mathbf{x}-\mathbf{y}|) d\mathbf{y}.$$

- $w_\delta = \frac{1}{\delta^d} w\left(\frac{\cdot}{\delta}\right)$; w: a mollifier supported on $[-1,1]$.
- Least-squares solution:

$$\mathbf{u}^T = \left(\int_\Omega w_\delta(|\mathbf{x}-\mathbf{y}|) \nabla\varepsilon(\mathbf{y}) \nabla\varepsilon^T(\mathbf{y}) d\mathbf{y} \right)^{-1} \int_{\mathbf{x}+\delta B} \mathrm{data} w_\delta(|\mathbf{x}-\mathbf{y}|) \nabla\varepsilon(\mathbf{y}) d\mathbf{y}.$$

- If all vectors $\nabla\varepsilon$ in $\{\mathbf{y} \; : \; w_\delta(|\mathbf{y}-\mathbf{x}|) \neq 0\}$ not collinear, then

$$\int_\Omega w_\delta(|\mathbf{x}-\mathbf{y}|) \nabla\varepsilon(\mathbf{y}) \nabla\varepsilon^T(\mathbf{y}) d\mathbf{y} \quad \text{invertible.}$$

- Resolution $=$ variation of ε.

Full-field optical coherence elastography

Optical image ε of the medium:

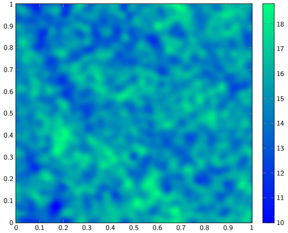

Full-field optical coherence elastography

Averaging kernel w_δ:

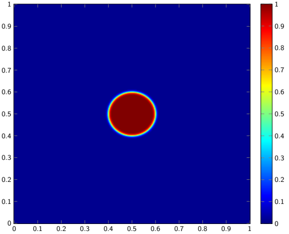

Conditioning of the matrix $w_\delta \star \nabla\varepsilon\nabla\varepsilon^T$:

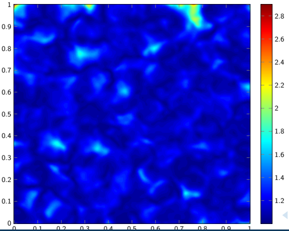

Full-field optical coherence elastography

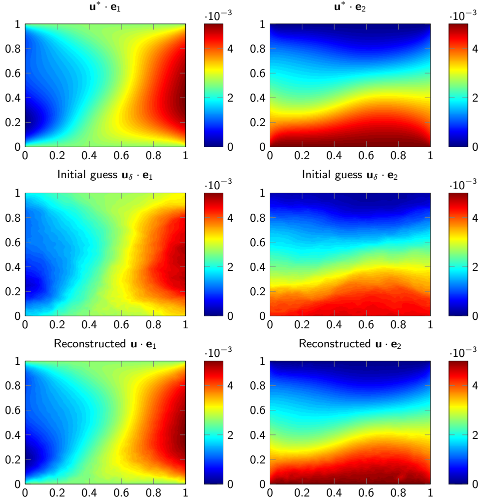

Displacement field and its reconstruction.

Full-field optical coherence elastography

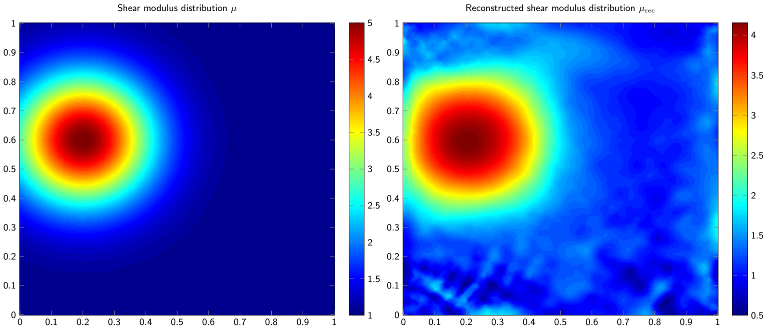

Shear modulus reconstruction.

Spectroscopic electrical tissue property imaging

- Differentiate between normal, pre-cancerous and cancerous tissues from electrical measurements at tissue level.
- Frequency dependence of the (anisotropic) homogenized admittivity: $\omega \mapsto K^*(\omega)$.
- Relaxation times:
  - $1/ \arg\max_\omega$ eigenvalues of $\Im m\, K^*(\omega)$;
  - Classification: invariance properties;
  - Measure of anisotropy: ratios of the eigenvalues of $\Im m\, K^*(\omega)$.

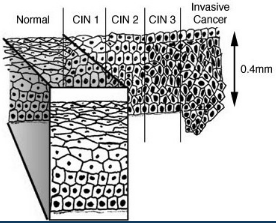

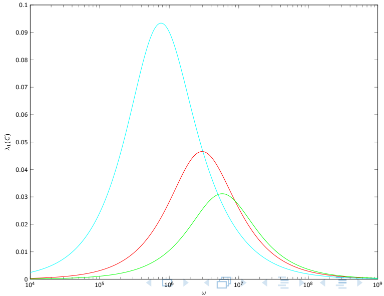

Spectroscopic electrical tissue property imaging

- Cell: homogeneous core covered by a thin membrane of contrasting electric conductivities and permittivities.
    - Intra and extra-cellular media: $k_0 := \sigma_0 + i\omega\varepsilon_0$ (conducting effect; transport of charges);
    - Membrane: $k_m := \sigma_m + i\omega\varepsilon_m$ with $\sigma_m/\sigma_0 \ll 1$ (capacitance effect; storage or charges or rotating molecular dipoles);
    - Thickness of the membrane $\ll$ typical size of the cell.

Spectroscopic electrical tissue property imaging

$$
\begin{cases}
-\nabla \cdot k_0 \nabla u_\delta^+ = 0 & \text{in } \Omega_\delta^+ \cup \Omega_\delta^-, \\
k_0 \dfrac{\partial u_\delta^+}{\partial n} = k_0 \dfrac{\partial u_\delta^-}{\partial n} & \text{on } \Gamma_\delta, \\
u_\delta^+ - u_\delta^- - \delta\, \xi \dfrac{\partial u_\delta^+}{\partial n} = 0 & \text{on } \Gamma_\delta, \\
\dfrac{\partial u_\delta^+}{\partial n} = g & \text{on } \partial\Omega.
\end{cases}
$$

- $u_\delta = u_\delta^\pm$ in $\Omega_\delta^\pm$;
- $\xi = \text{thickness} \times k_m / k_0$: effective thickness;
- g: electric field applied at $\partial\Omega$ of frequency ω ($\int_{\partial\Omega} g d\sigma = 0$).

Spectroscopic electrical tissue property imaging

The effective admittivity of a periodic dilute suspension[5]:

$$K^* = k_0 \left(I + f M \left(I - \frac{f}{2} M \right)^{-1} \right) + o(f^2).$$

- f: volume fraction; ξ: effective thickness of the membrane; ∂D: cell membrane; $\widetilde{D} = D/\sqrt{f}$: rescaled cell.
- M: membrane polarization tensor

$$M = - \left(\xi \int_{\partial \widetilde{D}} \nu_j \left(I + \xi L_{\widetilde{D}} \right)^{-1} [\nu_i](y) ds(y) \right)_{i,j=1,2}.$$

- $L_{\widetilde{D}}[\varphi](x) = \frac{1}{2\pi} \mathrm{p.v.} \int_{\partial \widetilde{D}} \frac{\partial^2 \ln |x-y|}{\partial \nu(x) \partial \nu(y)} \varphi(y) ds(y), \quad x \in \partial \widetilde{D}.$

[5] with J. Garnier, L. Giovangigli, W. Jing, J.K. Seo, J. Math. Pures Appl., 2016.

Spectroscopic electrical tissue property imaging

- Properties of the membrane polarization tensor:
  - M: symmetric; invariant by translation;
  - $M(sC,\xi) = s^2 M(C, \frac{\xi}{s})$ for any scaling parameter $s > 0$.
  - $M(\mathcal{R}C,\xi) = \mathcal{R}M(C,\xi)\mathcal{R}^t$ for any rotation $\mathcal{R}$.
  - $\Im m\, M$ is positive and its eigenvalues, $\lambda_1 \geq \lambda_2$, have one maximum with respect to ω.
- Relaxation times for the arbitrary-shaped cells:

$$\frac{1}{\tau_i} := \arg\max_{\omega} \lambda_i(\omega).$$

- $(\tau_i)_{i=1,2}$: invariant by translation, rotation and scaling.
- Concentric circular-shaped cells: Maxwell-Wagner-Fricke formula $(\lambda_1 = \lambda_2)$.
- Nondilute regime: Assume f known $\Rightarrow$ Classification based on relaxation times.

Plasmonic resonant nanoparticles

- Gold nano-particles: accumulate selectively in tumor cells; bio-compatible; reduced toxicity.
- Detection: localized enhancement in radiation dose (strong scattering).
- Ablation: localized damage (strong absorption).
- Functionalization: targeted drugs.

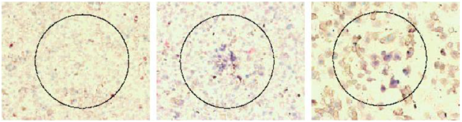

M.A. El-Sayed et al.

Plasmonic resonances for nanoparticles

- Spectral decomposition: (l, m)-entry

$$M_{l,m}(\lambda(\omega), D) = \sum_{j=1}^{\infty} \frac{(\nu_m, \varphi_j)_{\mathcal{H}^*} (\nu_l, \varphi_j)_{\mathcal{H}^*}}{(1/2 - \lambda_j)(\lambda(\omega) - \lambda_j)}.$$

- $(\nu_m, \varphi_0)_{\mathcal{H}^*} = 0$; φ_0: eigenfunction of $\mathcal{K}_D^*$ associated to $1/2$.
- Quasi-static far-field approximation[6]: $\delta \to 0$,

$$u^s = -\delta^d M(\lambda(\omega), B) \nabla_z G_{k_m}(x - z) \cdot \nabla u^i(z) + O\left(\frac{\delta^{d+1}}{\mathrm{dist}(\lambda(\omega), \sigma(\mathcal{K}_D^*))}\right).$$

- Quasi-static plasmonic resonance: $\mathrm{dist}(\lambda(\omega), \sigma(\mathcal{K}_D^*))$ minimal ($\Re e\, \varepsilon_c(\omega) < 0$).

[6] with P. Millien, M. Ruiz, H. Zhang, Arch. Ration. Mech. Anal., 2017.

Plasmonic resonances for nanoparticles

- $M(\lambda(\omega), B) = (\frac{\varepsilon_c(\omega)}{\varepsilon_m} - 1)\int_B \nabla v(y)dy$:

$$\begin{cases} \nabla\cdot\Big(\varepsilon_m \chi(\mathbb{R}^d \setminus \bar{B}) + \varepsilon_c(\omega)\chi(\overline{B})\Big)\nabla v = 0, \\ v(y) - y \to 0, \qquad |y| \to +\infty. \end{cases}$$

- Corrector v:

$$v(y) = y + \mathcal{S}_B(\lambda(\omega)I - \mathcal{K}_B^*)^{-1}[\nu](y), \quad y \in \mathbb{R}^d.$$

- Inner expansion: $\delta \to 0$, $|x - z| = O(\delta)$,

$$u(x) = u^i(z) + \delta v(\frac{x-z}{\delta}) \cdot \nabla u^i(z) + O(\frac{\delta^2}{\mathrm{dist}(\lambda(\omega), \sigma(\mathcal{K}_D^*))}).$$

- Monitoring of temperature elevation due to nanoparticle heating[7]:

$$\begin{cases} \rho C \frac{\partial T}{\partial t} - \nabla \cdot \tau \nabla T = \frac{\omega}{2\pi}(\Im(\varepsilon_c(\omega))\, |u|^2 \chi(D), \\ T|_{t=0} = 0. \end{cases}$$

ρ: mass density; C: thermal capacity; τ: thermal conductivity.

[7] with F. Romero, M. Ruiz, SIAM MMS, 2018.

Plasmonic resonances for nanoparticles

- Scattering amplitude:

$$u^s(x) = -ie^{-\frac{\pi i}{4}} \frac{e^{ik_m|x|}}{\sqrt{8\pi k_m|x|}} A_\infty[D, \varepsilon_c, \varepsilon_m, \omega](\theta, \theta') + o(|x|^{-\frac{1}{2}}),$$

$|x| \to \infty$; θ, θ': incident and scattered directions.

- Scattering cross-section:

$$Q^s[D, \varepsilon_c, \varepsilon_m, \omega](\theta') := \int_0^{2\pi} \Big| A_\infty[D, \varepsilon_c, \varepsilon_m, \omega](\theta, \theta') \Big|^2 d\theta.$$

- Enhancement of the absorption and scattering cross-sections Q^a and Q^s at plasmonic resonances[8]:

$$Q^a + Q^s (= \text{extinction cross-section } Q^e) \propto \Im m\, \mathrm{Trace}(M(\lambda(\omega), D));$$

$$Q^s \propto \Big| \mathrm{Trace}(M(\lambda(\omega), D)) \Big|^2.$$

[8] with P. Millien, M. Ruiz, H. Zhang, Arch. Ration. Mech. Anal., 2017.

Single particle imaging

- Single nanoparticle imaging[9]:

$$\max_{z^S} I(z^S, \omega)$$

- $I(z^S, \omega)$: imaging functional; z^S: search point.
- Resolution: limited only by the signal-to-noise-ratio.
- Cross-correlation techniques: robustness with respect to medium noise.

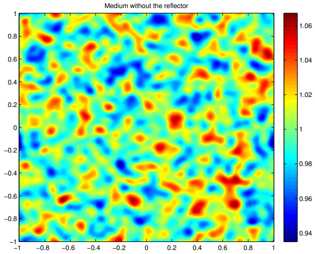

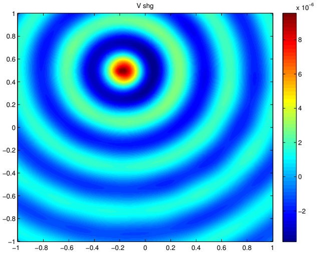

[9]with J. Garnier, P. Millien, SIAM J. Imag. Sci., 2014.

Concluding remarks

- Scale separation techniques, multi-wave imaging, single particle imaging.
- Source[10] and dynamic separation techniques[11].
- Functional conductivity imaging: Neuro-activity: localized conductivity change. Inject a dc current through electrodes and measure the change in the current density.
- Stem cells monitoring and tissue engineering: Image each layer and measure noninvasively its composition.

---

[10] with G.S. Alberti, ACHA, 2017.

[11] with G.S. Alberti, F. Romero, T. Wintz, submitted, 2018.